



OPEN

# Adropin ameliorates reproductive dysfunctions in letrozole-induced PCOS mouse

Shweta Maurya<sup>1</sup>, Shashank Tripathi<sup>1</sup>, Taruna Arora<sup>2</sup> & Ajit Singh<sup>1</sup>  

Polycystic ovary syndrome (PCOS) is the most common cause of infertility in reproductive-age women, and its etiology and exact treatment are not yet established. Adropin is a unique hepatokine involved in maintaining energy homeostasis, and its level has been reported to decline in serum and follicular fluid of PCOS women. Thus, present study was designed to investigate the effect of adropin on hormonal and reproductive abnormalities in PCOS mice. PCOS was induced in adult mice by administering letrozole (6 mg/kg body weight) orally for 21 days. PCOS mice were subsequently treated with adropin (450 nmol/kg body weight) for 15 days. Adropin treatment drastically decreased serum testosterone by suppressing the ovarian expression of 17 $\beta$ -HSD in PCOS mice. It also improved the follicular proliferation and survival by enhancing the ovarian expression of PCNA and BCL2 and suppressing the BAX, cleaved caspase 3, and TUNEL-positive cells in PCOS mice. Most of the effects of adropin are comparable to metformin (current PCOS treatment). Notably, adropin shows more efficacy than metformin in treating reproductive abnormalities in PCOS mice, as evidenced by early regularization of cyclicity and enhanced ovarian expression of 3 $\beta$ -HSD and aromatase proteins. Thus, adropin may be an alternative therapeutic option for managing PCOS.

**Keywords** Adropin, GPR19, Metformin, PCOS, Fertility

Polycystic ovary syndrome (PCOS) is a common endocrine disorder that affects women of reproductive age, with a prevalence of 6–15% globally<sup>1,2</sup>. This endocrinopathy is associated with several reproductive and metabolic disorders, including ovulatory dysfunction, menstrual abnormalities, aberrant follicular development, endometrial hyperplasia, reduced fertility, insulin resistance, dyslipidemia, diabetes mellitus, and coronary artery diseases<sup>3–5</sup>. The Rotterdam diagnostic criteria of PCOS require the presence of at least two out of the three features, including hyperandrogenism, chronic anovulation, and polycystic ovaries<sup>6</sup>. Despite being diagnosed in 1935, the exact cause of PCOS remains elusive. Therefore, treatment is symptomatic which comprises metformin, clomiphene citrate, combined oral contraceptive pills, weight loss surgery, and lifestyle changes<sup>7,8</sup>. Metformin alleviates insulin resistance and obesity and is linked to regular menstrual cyclicity, enhanced ovulation, and lowered circulating androgen levels and thus plays a significant role in the management of PCOS<sup>9–11</sup>.

Several organokines derived from adipose tissue, liver, and skeletal muscles are involved in energy metabolism and reproductive functions. The plasma concentrations of adiponectin<sup>12</sup>, resistin<sup>13,14</sup>, visfatin<sup>15,16</sup>, omentin<sup>17,18</sup>, chemerin<sup>19,20</sup> and apelin<sup>21</sup> exhibit variability among women with PCOS. Nevertheless, the role of adropin, a hepatokine, in ovarian pathophysiology is not well understood.

Adropin is a peptide hormone that maintains energy homeostasis<sup>22</sup>. Inadequate amounts of adropin are associated with insulin resistance, impaired fasting glucose, and dyslipidemia<sup>23</sup>. Adropin affects muscles, liver, and adipose tissue to regulate glucose and fatty acid metabolism. In skeletal muscle, adropin enhances the insulin signaling pathways by increasing the Akt phosphorylation and cell surface translocation of GLUT4, thereby facilitating the absorption of glucose mediated by insulin<sup>24</sup>. In the liver, adropin lowers hepatic glucogenesis and suppresses the expression of fatty acid import proteins and gluconeogenic enzymes, thus improving insulin sensitivity<sup>25</sup>. Moreover, adropin enhances cardiac efficiency and cardiac insulin sensitivity by suppressing fatty acid oxidation and promoting glucose oxidation in the heart<sup>26</sup>. Adropin reduces adipogenesis and lipid synthesis and storage by suppressing the expression of adipogenic and lipogenic genes, as well as intracellular lipid content<sup>27</sup>.

Adropin has been reported to enhance gonadal activity in both male and female mice<sup>28–33</sup>. However, a limited number of reports are available on the role of adropin in PCOS pathophysiology. PCOS women have lower levels of adropin in both their serum and follicular fluid compared to normal women<sup>34</sup>. Another study stated that lower

<sup>1</sup>Department of Zoology, Institute of Science, Banaras Hindu University, Varanasi 221005, India. <sup>2</sup>RCN Division, ICMR, New Delhi 110029, India. ✉email: ajitsinghrepro@gmail.com

adropin levels in PCOS women are linked to higher levels of inflammatory marker,  $\text{TNF-}\alpha^{35}$ . Nevertheless, these researches failed to elucidate the intricate correlation between adropin levels and the pathophysiology of PCOS. An extensive investigation is required to establish the relationship between adropin and PCOS pathogenesis, which will offer insights and direction for the development of novel therapeutic strategies.

Hence, the primary aim of this study was to investigate the impact of adropin on hormonal and reproductive dysfunctions in letrozole-induced PCOS mice. Additionally, the impact of the adropin was compared to that of metformin on PCOS mice, to provide an ideal therapeutic option for PCOS patients.

## Results

### Adropin expression decreases in the ovary of PCOS mice

The cellular localization of adropin in the ovaries of vehicle-treated control (VC) and PCOS mice was examined by using immunohistochemistry. The ovary of VC mice showed very strong immunoreactivity of adropin in the corpus luteum (CL), while moderate to mild immunoreactivity was noted in the theca-interstitial cells (TICs), granulosa cells (GCs), and oocytes (Fig. 1A–C). However, the letrozole-induced PCOS mice showed moderate immunostaining in the TICs, and mild immunostaining in the GCs and oocytes (Fig. 1D–F).

Furthermore, the change in the ovarian expression of adropin was examined by immunoblotting followed by densitometry. The ovarian expression of adropin was found to be significantly ( $p < 0.01$ ) decreased in the PCOS group as compared to the VC (Data in supplementary file).

### Adropin treatment regularizes the estrous cycle of PCOS mice

The VC mice showed regular estrous cycles having proestrus, estrus, metestrus, and diestrus phases throughout the experiment (Fig. 2A, D). The letrozole-treated PCOS mice showed irregular estrous cycles after the first two cycles and thereafter stayed in a persistent diestrus phase (Fig. 2B, E). However, in the PCOS + ADR group, the diestrus phase of estrous cycle was regularized after day 7 of adropin treatment (Fig. 2F). In the case of metformin administration in the PCOS mice, we observed the estrus phase on the 10th day of treatment. (Fig. 2G). Overall, the administration of adropin in PCOS mice resulted in early restoration of estrous cycle compared to that of the metformin-treated PCOS group. (Table 1)

### Adropin treatment restores ovarian morphology in PCOS mice

PCOS mice exhibited a significant ( $p < 0.001$ ) decrease in ovary mass compared to the VC mice. However, the ovary mass was significantly increased upon the treatment of both adropin and metformin in the PCOS mice compared with the untreated PCOS mice (Fig. 3A, B).

Histological ovarian sections of the VC mice showed the presence of large CL as well as numerous small and large antral follicles (Fig. 3C–F). These antral follicles contained normal healthy GCs, TICs, and oocytes (Fig. 3E). In contrast, the PCOS mice showed the presence of numerous cystic follicles, few atretic follicles, and complete absence of CL (Fig. 3G–I). The follicles are comprised of a thin layer of sparsely distributed GCs and a large cystic antral cavity (Fig. 3I). Interestingly, the adropin-treated PCOS mice showed healthy antral follicles consisting of thick layers of densely aggregated GCs, and CL, while the cystic follicles were completely absent (Fig. 3J–M). However, the metformin-treated PCOS mice showed the presence of healthy antral follicles and few atretic follicles (Fig. 3N–P).

### Immunolocalization and ovarian expression of cell proliferation (PCNA) protein

Immunohistochemical localization of PCNA in the VC ovary showed strong immunoreactivity in the majority of GCs of the ovarian follicles (Fig. 4A). Conversely, very weak immunoreactivity in only a few GCs of ovarian follicles was noted in the histological sections of the PCOS ovary (Fig. 4B). However, both adropin (Fig. 4C) and metformin-treated (Fig. 4D) PCOS ovaries showed intense PCNA immunoreactivity in most of the GCs within the ovarian follicles as compared to the untreated PCOS ovary.

Furthermore, densitometric analysis of PCNA immunoblot showed a significantly ( $p < 0.01$ ) decreased expression in the PCOS group as compared to the VC group. In contrast, a significant elevation was noted in the expression of PCNA in PCOS + ADR and PCOS + MET groups, as compared to the untreated PCOS group (Data in supplementary file).

### Ovarian expression of cell survival and apoptosis-related proteins by Western blotting

The densitometric analysis of the Western blot of BCL2 revealed a significant ( $p < 0.001$ ) reduction in the ovary of PCOS group when compared to the VC group. However, its expression was noted to increase significantly in both PCOS + ADR and PCOS + MET groups compared to untreated PCOS group (Fig. 5A). The ovarian expression of apoptotic proteins [BAX (Fig. 5A) & cleaved caspase3 (Fig. 5C)] and the ratio of BAX/ BCL2 (Fig. 5B) & cleaved caspase 3/ caspase 3 (Fig. 5D) were significantly increased in the PCOS group as compared to the VC group. However, both adropin and metformin-treated PCOS groups showed significant ( $p < 0.05$ ) reduction in expression of BAX & cleaved caspase 3, and the ratio of BAX/BCL2 & cleaved caspase 3/ caspase 3 as compared to the untreated PCOS group.

The densitometric analysis of the immunoblots of receptor protein, GPR19, showed a significant ( $p < 0.05$ ) decreased expression in the PCOS group as compared to the VC group. However, both adropin and metformin-treated PCOS groups showed significant ( $p < 0.05$ ) elevation in the ovarian expression as compared to the untreated PCOS group (Data in supplementary file).

### Evaluation of apoptosis in the ovaries by TUNEL assay

The apoptotic cells within the ovarian histological sections of VC, untreated PCOS, and treated PCOS (adropin and metformin) groups were detected by performing the TUNEL assay. In the case of VC (Fig. 5E, F), and both



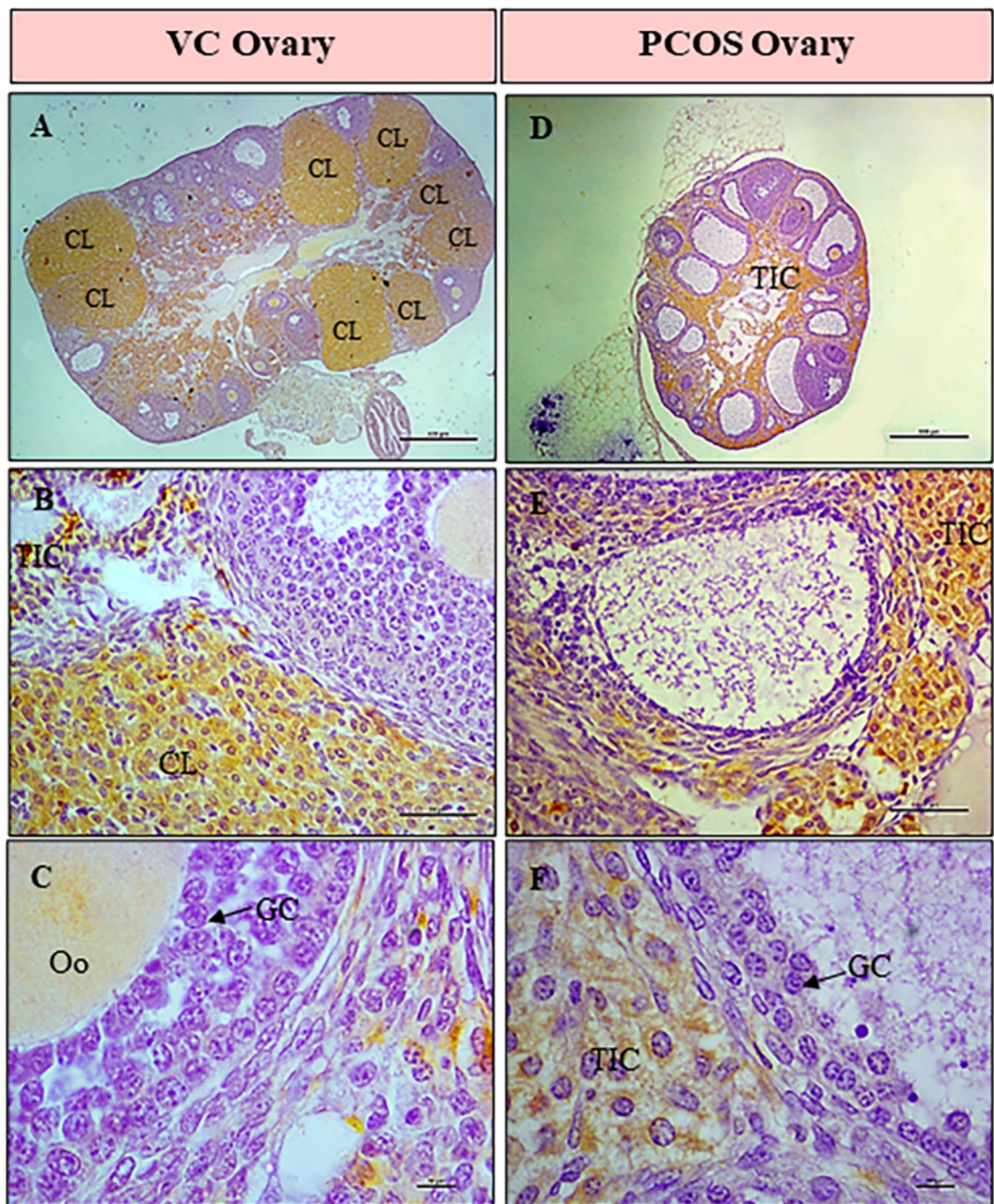


**Fig. 1.** Ovarian expression of Adropin in VC and PCOS mice. (A–C) Representative histological sections showing strong adropin immunoreactivity in the CL, while moderate immunoreactivity in the TICs of the VC ovary. (D–F) Moderate adropin immunoreactivity is noted in the TICs of PCOS ovary. (A) and (D) are shown at 10x magnification, (B) and (E) are shown at 40x magnification whereas (C) and (F) are shown at 100x magnification. VC vehicle-treated control, PCOS polycystic ovary, CL corpus luteum, Oo oocyte, GC granulosa cell, TIC Theca interstitial cell.



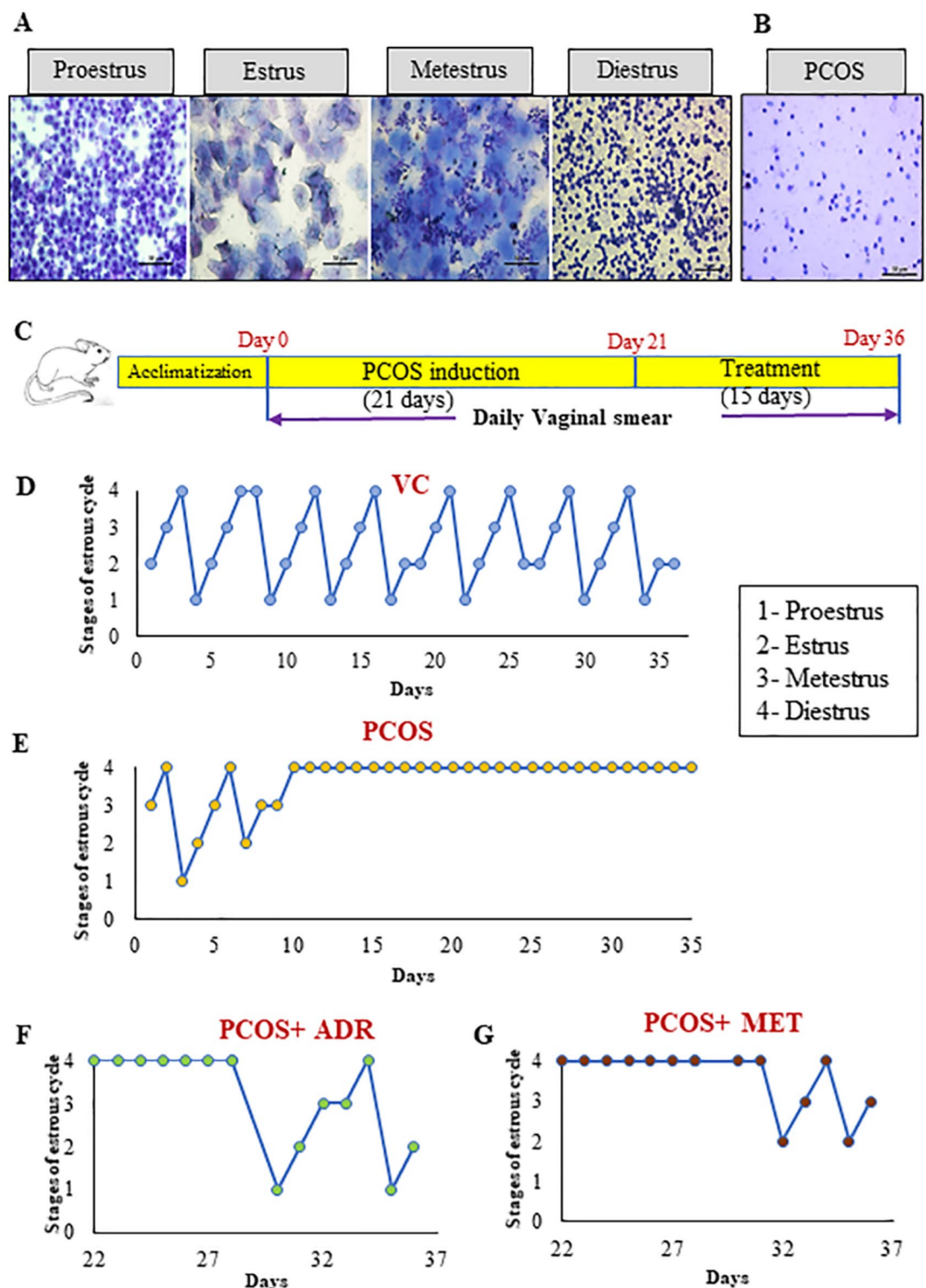


**Fig. 2.** Vaginal smear and estrous cycle pattern in VC, PCOS, PCOS+ADR and PCOS+MET mice. **(A)** Representative vaginal smears from the VC mice showing different estrous cycle phases including proestrus with nucleated epithelium, estrus with cornified epithelium, metestrus with both cornified epithelium and neutrophils, and diestrus with neutrophils. **(B)** Representative vaginal smear from the PCOS mice showing the diestrus phase. **(C)** Schematic diagram showing animal experimentation. **(D)** The normal estrous cycle of the VC mice. **(E)** Persistent diestrus phase of the estrous cycle in the PCOS mice. Recovery of the estrous cycle in **(F)** PCOS+ADR mice and **(G)** PCOS+MET mice. VC vehicle-treated control mice, PCOS polycystic mice, PCOS+ADR adropin-treated PCOS mice, PCOS+MET metformin-treated PCOS mice.

Groups	Average no. of cycles after treatment with adropin/metformin
VC	3.1 ± 0.2
PCOS	0 ± 0 <sup>†b</sup>
PCOS + ADR	1.6 ± 0.3 <sup>-b</sup>
PCOS + MET	1.06 ± 0.11 <sup>*a</sup>

**Table 1.** Effects of Adropin or Metformin treatment on estrous cycle of PCOS mice. Data are expressed as mean ± SEM (*n* = 3/group) and were analyzed by one-way ANOVA followed by the post hoc Bonferroni test. <sup>†</sup>VC versus PCOS. <sup>-</sup>PCOS versus PCOS + ADR. <sup>\*</sup>PCOS versus PCOS + MET. <sup>a</sup>*p* < 0.01. <sup>b</sup>*p* < 0.001.

PCOS + ADR (Fig. 5I, J) & PCOS + MET (Fig. 5K, L) ovaries, very few brown-coloured TUNEL-positive GCs were observed. In contrast, the ovarian follicles of the PCOS ovary showed a high number of TUNEL-positive cells as compared to other experimental groups (Fig. 5G, H). The TUNEL-positive reaction was mainly observed in the layer of GCs located at the side of the antrum of the cystic follicles (Fig. 5H).

**Changes in Circulating hormone levels and ovarian expression of steroidogenic proteins**

The concentration of circulating progesterone (Fig. 6A) and testosterone (Fig. 6B) were significantly (*p* < 0.05) increased, while estradiol (Fig. 6C) was significantly (*p* < 0.05) decreased in PCOS mice as compared to the VC mice. However, PCOS + ADR mice exhibited a significant (*p* < 0.05) elevation in serum P4 levels, while experiencing a significant (*p* < 0.05) reduction in T levels as compared to the untreated PCOS mice. On the other hand, a significant decrease in both P4 and T levels were noted in PCOS + MET mice as compared to the untreated PCOS mice. In case of serum E2, no significant change was noticed in both PCOS + ADR and PCOS + MET mice as compared to untreated PCOS mice.

Furthermore, ovarian expression of steroidogenic markers (StAR, CYP11A1, 3β-HSD, 17β-HSD, and aromatase) were determined by immunoblotting followed by densitometry (Fig. 6D). The expression of StAR, CYP11A1, and 17β-HSD proteins was found to be significantly (*p* < 0.05) increased in PCOS ovaries, but there was no significant change in the expression of 3β-HSD and aromatase proteins compared to VC ovaries. In the PCOS + ADR group, there was a significant (*p* < 0.05) elevation in the ovarian expression of StAR, 3β-HSD, and aromatase proteins, whereas the expression of 17β-HSD was significantly reduced compared to the untreated PCOS group. In addition, we noticed a significant reduction in ovarian expression of StAR, CYP11A1, 17β-HSD, and aromatase proteins in the PCOS + MET mice, but there was no considerable change in ovarian expression of 3β-HSD protein compared to the untreated PCOS mice.

**Evaluation of fertility**

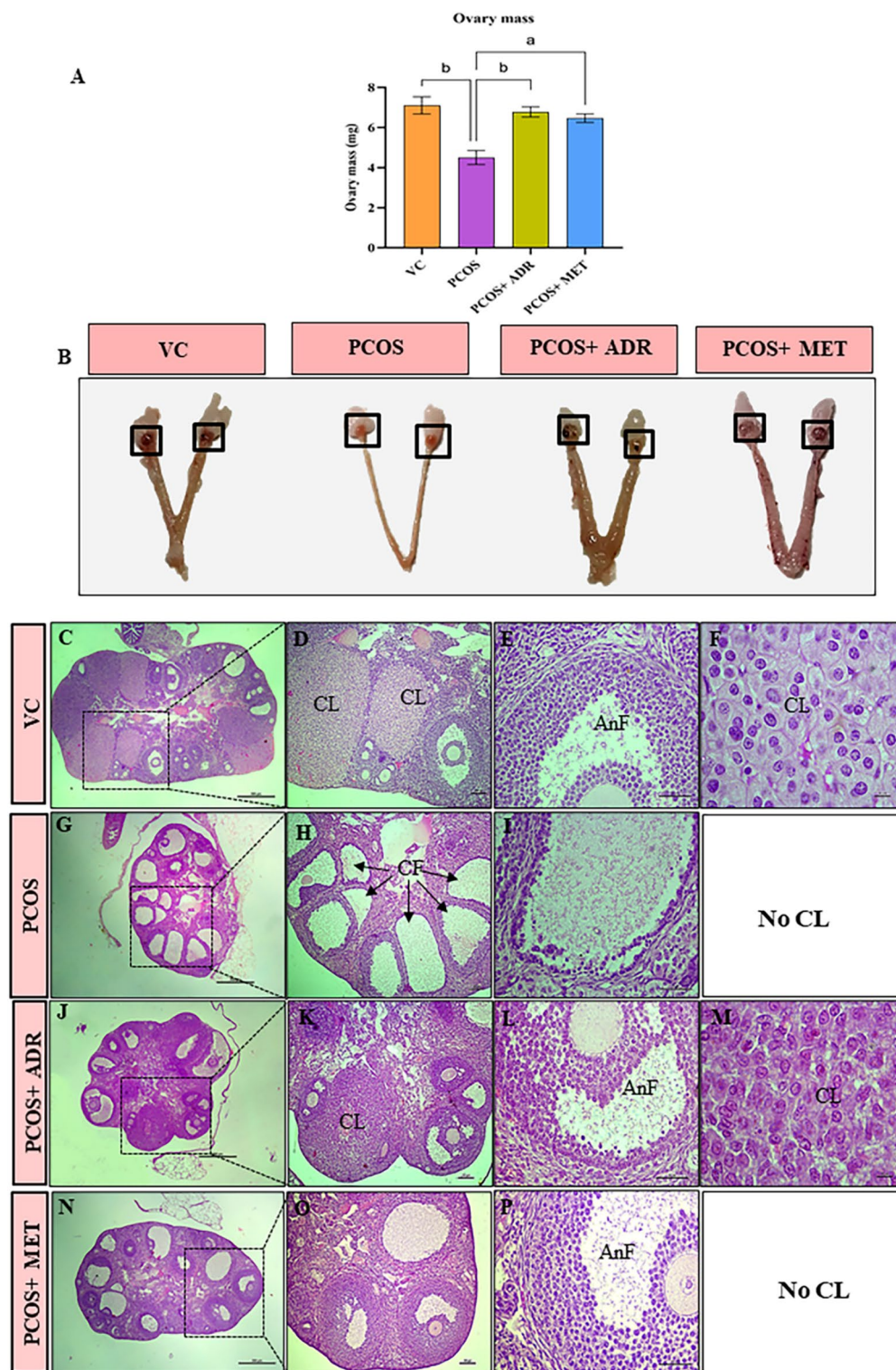
The fertility in the PCOS mice is severely impaired as none of them displayed any implantation sites in their uterine horns after 10 days of mating. However, PCOS mice treated with adropin and metformin showed embryo implants in their uterine horns, indicating the restoration of fertility (Fig. 7).

**Discussion**

PCOS is a chronic multisystem disorder of unknown etiology. Currently, no authorized medicine exists specifically for treating PCOS. Symptom-oriented medications are implemented to restore metabolic and reproductive functions in PCOS women. So, the current study is an attempt to examine the effect of adropin on hormonal and reproductive dysfunctions in PCOS mice that may provide an alternative therapeutic option for the management of PCOS. Mice were treated with letrozole to induce PCOS-like features such as increased levels of circulating testosterone, development of numerous ovarian cystic follicles, and absence of ovulation, as evidenced by lack of CL in the ovary. Immunohistochemical study showed significant alteration in the abundance of adropin immunoreactivity in the ovary of PCOS mice. VC ovaries showed the presence of numerous healthy ovarian follicles and CL and strong to moderate immunoreactivity of adropin was seen in the CL and TICs. However, as PCOS ovaries lack CL, moderate adropin immunoreactivity was seen in TICs only. Additionally, immunoblot analyses showed a decrease in the ovarian expression of adropin in PCOS as compared to VC. Recently, we have reported the strong immunoreactivity of adropin in CL of adult mice<sup>31,32</sup>. Recent clinical research has revealed reduced levels of adropin in the serum and follicular fluid of women with PCOS<sup>34</sup>. Altogether, IHC and immunoblot analyses demonstrated decreased ovarian adropin expression in PCOS condition. So, based on these findings, it is tempting to hypothesized that decreased adropin expression may be responsible for the degenerative changes in the ovary of PCOS mice and adropin treatment may restore the ovarian function of PCOS mice.

In order to find out the impact of adropin, PCOS mice were treated either with adropin or metformin (current PCOS treatment, positive control). Adropin is a well-known insulin sensitizer. It enhances insulin-induced glucose uptake in the skeletal muscles by sensitizing insulin signalling pathway<sup>24</sup>. In the liver, adropin is reported to antagonize the glucagon signalling pathway and reduces hepatic glucose level by sharing the same molecular mechanism as the metformin<sup>36</sup>.

Adropin treatment in PCOS mice regularized the estrous cycle, increased the ovary mass, and restored the normal ovarian morphology characterized by absence of cystic follicle and presence of healthy ovarian follicles and CL (indicator of ovulation). Similarly, the acyclic PCOS mice that received metformin regained their cyclicity, and their ovaries exhibited a healthy morphological condition. Earlier research has also documented



that metformin improves the regularity of menstrual cycles in PCOS patients<sup>9</sup>. Nevertheless, treatment with adropin in PCOS mice resulted in early restoration of estrous cycles compared to the metformin-treated group.

It is widely recognized that hyperandrogenism is closely associated with the majority of the metabolic and reproductive abnormalities of PCOS<sup>37</sup>. Around 75–90% of PCOS women with oligomenorrhea experience high androgen levels<sup>38,39</sup>. Our study revealed, both, adropin as well as metformin administration in PCOS mice significantly declined the circulating testosterone levels by suppressing the ovarian expression of 17 $\beta$ -HSD activity, thereby reducing the theca cell steroidogenesis. 17 beta-hydroxysteroid dehydrogenase (17 $\beta$ -HSD) enzyme is responsible for the conversion of androstenedione to testosterone<sup>40</sup>. Of note, adropin treatment to PCOS mice significantly increased the level of P4, a hormone involved in the process of ovulation. In our recent report, we have established the role of adropin in increased P4 production and maintenance of CL function in mice<sup>31,33</sup>. In progesterone receptor knockdown mice, oocyte is trapped into luteinized follicles resulting into



◀ **Fig. 3.** Ovary mass and histoarchitectural changes in different experimental groups. **(A)** Effect of exogenous treatment of adropin and metformin on ovary mass. **(B)** Representative photographs of the ovary with uterus of the mice of different experimental groups. Data are expressed as mean  $\pm$  SEM ( $n = 3$ ) and were analyzed by one-way ANOVA followed by the post hoc Bonferroni test. **(C–F)** Representative images of VC mice ovary; **(C)** ovarian section showing the presence of large CL as well as numerous small and large antral follicles; **(D)** healthy ovarian follicles with the presence of CL; **(E)** Antral follicle (AnF) with healthy GCs and oocyte (Oo); **(F)** luteal cells of the CL. **(G–I)** Representative images of PCOS mice ovary; **(G)** ovarian section showing presence of numerous cystic follicles (CF) and absence of CL; **(H)** presence of numerous CFs with thin layers of GCs; **(I)** cystic follicle having a large antrum and sparsely distributed GCs. **(J–M)** Representative images of adropin-treated PCOS mice ovary; **(J)** section of the ovary showing healthy follicles and CL; **(K)** ovarian antral follicles and CL; **(L)** antral follicle with healthy GCs; **(M)** luteal cells of CL. **(N–P)** Representative images of metformin-treated PCOS mice ovary; **(N)** section of the ovary showing numerous antral follicles and few atretic follicles; **(O)** antral follicles with healthy GCs; **(P)** antral follicle showing densely aggregated GCs. **(C, G, J, N)** are shown at 4x magnification, **(D, H, K, O)** are shown at 10x magnification, **(E, I, L, and P)** are shown at 40x magnification whereas **(F, M)** are shown at 100x magnification. VC vehicle-treated control mice, PCOS polycystic mice, PCOS + ADR adropin-treated PCOS mice, PCOS + MET metformin-treated PCOS mice, CL corpus luteum, GC granulosa cell, Oo oocyte. <sup>a</sup> $p < 0.01$ ; <sup>b</sup> $p < 0.001$ .

failure of ovulation<sup>41</sup>. So, increased P4 in adropin treated mice is indicative of ovulation which is evident by presence of CL. Moreover, adropin treatment elevated while metformin treatment inhibited aromatase expression in PCOS-ovary. However, we did not observe a significant change in estradiol levels when we treated PCOS mice with adropin for 15 days. A longer duration of treatment may result in increased estradiol production. Various compounds including metformin have been reported to reduce the production of androgens in letrozole-induced PCOS mice<sup>42–49</sup>. Moreover, metformin therapy has been shown to effectively restore ovulation, regulate the menstrual cycle, and alleviate hirsutism, thus playing a crucial role in the management of PCOS<sup>11,50</sup>. Overall, similar to metformin, the administration of adropin to PCOS mice resulted in the normalization of hormonal levels and successful ovulation. Adropin treatment showed better efficacy than metformin in terms of increasing P4 production and aromatase expression.

Furthermore, the administration of adropin in PCOS mice resulted in a significant rise in the ovarian expression of GPR19 (adropin receptor), cell proliferation (PCNA) and survival (BCL2) markers, whereas decline in the expression of pro-apoptotic (BAX, and cleaved caspase 3) proteins and BAX/BCL2 ratio. IHC investigations revealed that administration of adropin in PCOS mice resulted in enhanced GC proliferation (PCNA) of healthy ovarian follicles, leading to an increase in follicular growth and ovarian mass. Moreover, elevated anti-apoptotic and reduced pro-apoptotic markers observed in adropin-treated PCOS mice suggest that adropin enhances the survival, growth, and development of healthy ovarian follicles by inhibiting degeneration and apoptosis of follicles. This was further validated by performing a TUNEL assay, which revealed very few TUNEL-positive GCs within the follicles of the adropin-treated PCOS mice. Hyperandrogenism has been reported to induce GCs apoptosis in PCOS<sup>51,52</sup>. Altogether these findings suggest that high androgen level increases apoptosis of GCs in PCOS mice while adropin as well as metformin treatment reduces T production thereby restoring the GCs proliferation and survival.

In addition, we also performed fertility test to evaluate the reproductive efficacy of PCOS mice after the administration of adropin or metformin. The PCOS mice showed no indications of pregnancy, indicating a state of complete infertility. However, adropin treatment in PCOS mice led to pregnancy similarly to the metformin therapy, as evidenced by the presence of embryo implants in their uterine horns. Hence, it can be concluded that adropin, exhibiting similar effect to metformin, has the capability to facilitate fertility in PCOS mice.

In summary, adropin treatment in PCOS mice significantly decreases 17 $\beta$ -HSD expression, resulting in decreased T production (a hallmark of PCOS). Adropin also increases P4 production that promotes ovulation, which is evident by the presence of CL in adropin-treated PCOS ovary. Decreased T in adropin-treated mice results in increased GC proliferation and survival and decreased apoptosis. It is worth mentioning that adropin treatment is more effective than metformin in restoring normal reproductive activity in PCOS mice, as evident by early regularization of the estrous cycle, enhanced P4 production, and ovarian expression of 3 $\beta$ -HSD and aromatase proteins. Therefore, adropin has the potential to be a promising alternative therapeutic option for managing PCOS.

## Methods

### Animal resources

Fifty-four adult Swiss strain female mice (weighing between 28 and 30 g) of 90 days old were purchased from the Department of Zoology, Institute of Science, Banaras Hindu University, Varanasi. The experiments were conducted at the standard temperature ( $25 \pm 2$  °C), relative humidity ( $50 \pm 5\%$ ), and on a light/dark cycle (12 h light/ 12 h dark). Mice were given commercial food pellets and water ad libitum. The animal ethical approval was provided by the Institutional Animal Ethical Committee, Institute of Science, Banaras Hindu University, Varanasi, India (BHU/ DoZ/IAEC/2019-20/034). The animal experiments were performed in accordance with ARRIVE guidelines. All methods were performed in accordance with the relevant guidelines.

### PCOS induction and drug administration

Mice were randomly divided into 2 groups: (i) vehicle-treated control mice (VC,  $n = 15$ ); (ii) PCOS mice (PCOS,  $n = 39$ ). PCOS was induced in the female *Mus musculus* (90-day-old) through oral administration of

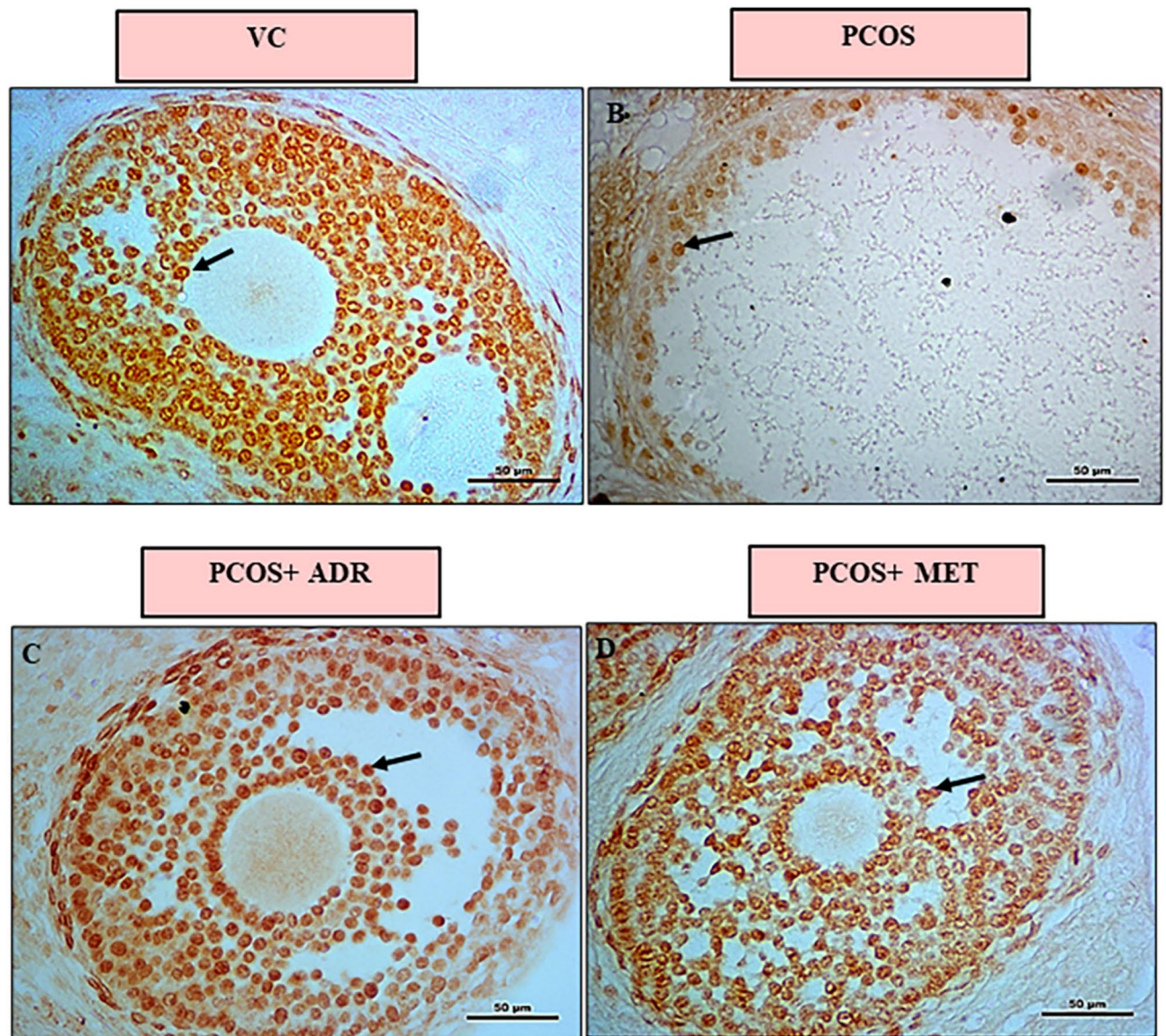


**Fig. 4.** Representative images of PCNA immunolocalization in the ovarian sections in different experimental groups. Arrowhead indicates nuclear PCNA immunostaining in GCs of ovarian follicle. (B) Antral follicle of PCOS ovary is showing few immunopositive GCs, whereas antral follicle of (A) VC, (C) PCOS + ADR, (D) PCOS + MET ovaries are showing the majority of PCNA immunopositive GCs. Figures (A–D) are shown in 40x magnification. VC vehicle-treated control mice, PCOS polycystic mice, PCOS + ADR adropin-treated PCOS mice, PCOS + MET metformin-treated PCOS mice.

letrozole (TCI India Pvt. Ltd.; Product no. L0248) at dosages of 6 mg/kg body weight, 100 µl/mouse in 0.5% carboxymethylcellulose (CMC) for consecutive 21 days<sup>53,54</sup>. Control mice received vehicle only (0.5% CMC) for the same period. The estrous cycle of each mouse was monitored during the entire course of treatment. 24 h after the last dose, 3 mice from both groups were sacrificed in mild anesthesia xylazine (8 mg/kg)/ ketamine (60 mg/kg) to verify PCOS-like features. The presence of PCOS in the mice treated with letrozole was validated according to the Rotterdam criteria<sup>6</sup>.

After the successful induction of the PCOS, the in vivo experiments were performed in four groups of mice ( $n = 12$  in each group): (i) vehicle-treated control mice (VC); (ii) PCOS mice; (iii) PCOS mice treated with adropin (450 nmol/kg b.w., intraperitoneal dose; PCOS + ADR); (iv) PCOS mice treated with metformin (500 mg/kg b.w., oral dose; PCOS + MET). The VC and PCOS mice were treated with distilled water, whereas mice in groups (iii) and (iv) were treated with adropin and metformin, respectively, for 15 consecutive days. The adropin peptide (NovoPro Biosciences Inc., Shanghai; Cat.#: 314322) dose was selected based on prior studies<sup>33,55</sup>. The dose of metformin (TCI India Pvt. Ltd.; Product no. M2009) was selected according to previous studies<sup>54,56</sup>. The estrous cycle of each mouse was monitored during the entire course of treatment. 9 mice from each group were sacrificed 24 h after the last dose. The serum was collected and stored at  $-20^{\circ}\text{C}$ . Three ovaries from each group were fixed in Bouin's fixative at room temperature. The other ovaries were cleaned, weighed, and



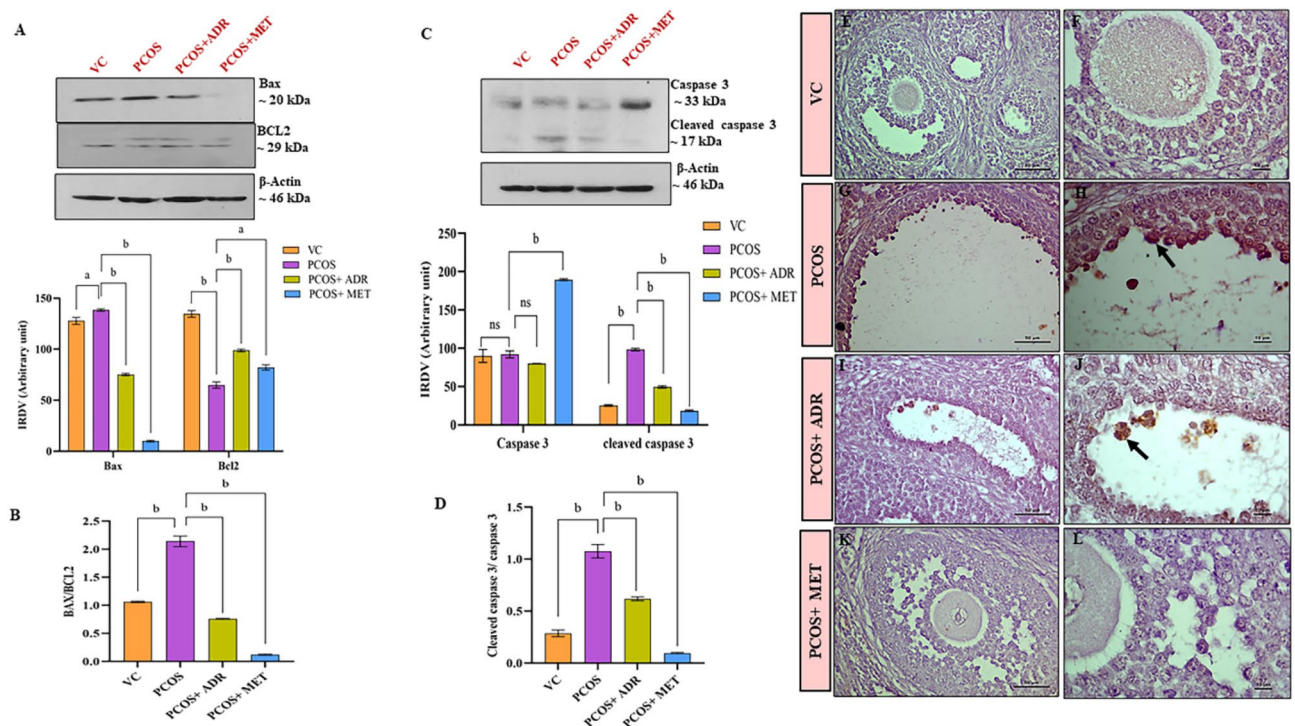


**Fig. 5.** Western blot analysis of apoptosis-related proteins and detection of apoptotic cells in ovarian sections of different experimental groups. **(A)** Representative immunoblots and densitometric analysis of ovarian BAX & BCL2; **(C)** Caspase 3 & cleaved caspase 3 protein expressions. **(B)** The bar graphs showing the ratio of BAX/BCL2; **(D)** Cleaved caspase3/caspase 3 in different experimental groups. Data are expressed as IRDV  $\pm$  SEM analyzed by one-way ANOVA followed by the post hoc Bonferroni test.  $\beta$ -actin is used to normalize the results of immunoblots. Representative histological sections showing the TUNEL-positive apoptotic cells in the ovary of **(E, F)** VC, **(G, H)** PCOS, **(I, J)** PCOS + ADR, and **(K, L)** PCOS + MET mice. Apoptotic granulosa cells are shown by an arrowhead. Figures **(A, C, E, G)** are shown in 40x magnification, whereas figures **(B, D, F, H)** are shown in 100x magnification. VC vehicle-treated control mice, PCOS polycystic mice, PCOS + ADR adropin-treated PCOS mice, PCOS + MET metformin-treated PCOS mice, IRDV integrated relative density value. <sup>a</sup> $p < 0.01$ ; <sup>b</sup> $p < 0.001$ ; ns—not significant.

stored at  $-80^{\circ}\text{C}$  for immunoblotting. The remaining 3 mice from each group were used for fertility assessment. A schematic diagram of experimental design is shown in Fig. 2C.

### Fertility assessment

After the end of the dosing (vehicle, adropin, or metformin), the 3 mice from each group were used for fertility assessment. 3 female mice from each group were housed with one fertile stud male mouse and left overnight. Vaginal plugs were checked the next morning (6:00 am) to confirm the mating. The day when the vaginal plug was observed was considered as Day 1. The mice were sacrificed on Day 10 by cervical dislocation, the uterus was removed to detect the implantation sites.

### Hormonal assay: progesterone (P4), estradiol (E2), and testosterone (T)

The concentrations of serum P4, T, and E2 were estimated by using a commercially available ELISA kit (Diametra, lot no. DKO006/ DKO002/ DKO003) according to the instructions given by the manufacturer. In brief, 20  $\mu\text{l}$  of standard/serum was taken in P4 ELISA wells. In the case of T and E2, 25  $\mu\text{l}$  of standard or serum were taken in wells of respective ELISA microplates. Subsequently, HRP-tagged conjugate solution was added to the wells of P4 (200  $\mu\text{l}$ ), E2 (200  $\mu\text{l}$ ), and T (100  $\mu\text{l}$ ) microplates. Thereafter, P4 and T ELISA plates were incubated for 1 h, whereas E2 for 2 h at  $37^{\circ}\text{C}$ . Afterwards, the contents were decanted from wells and washed three times with 300  $\mu\text{l}$  of diluted wash buffer. Then, 100  $\mu\text{l}$  of tetramethyl benzidine (TMB) chromogen substrate was added to each well. P4 and T microplates were incubated for 15 min, whereas E2 microplate was incubated for 30 min at room temperature in a dark chamber. Further, 100  $\mu\text{l}$  of stop solution (0.15 M sulfuric acid) was added to stop the reaction, and absorbance was taken at 450 nm within 5 min using a multimode microplate reader (Synergy H1; Biotek Instruments, USA).

### Histology

One ovary from each mouse ( $n=3/\text{group}$ ) was collected from all four experimental groups. The ovaries were cleaned from any adherent fat, weighed, and fixed in Bouin's fixative for 18–22 h at room temperature. Thereafter, ovaries were dehydrated in ascending grades of ethanol (70%, 90%, and absolute), cleared in xylene,

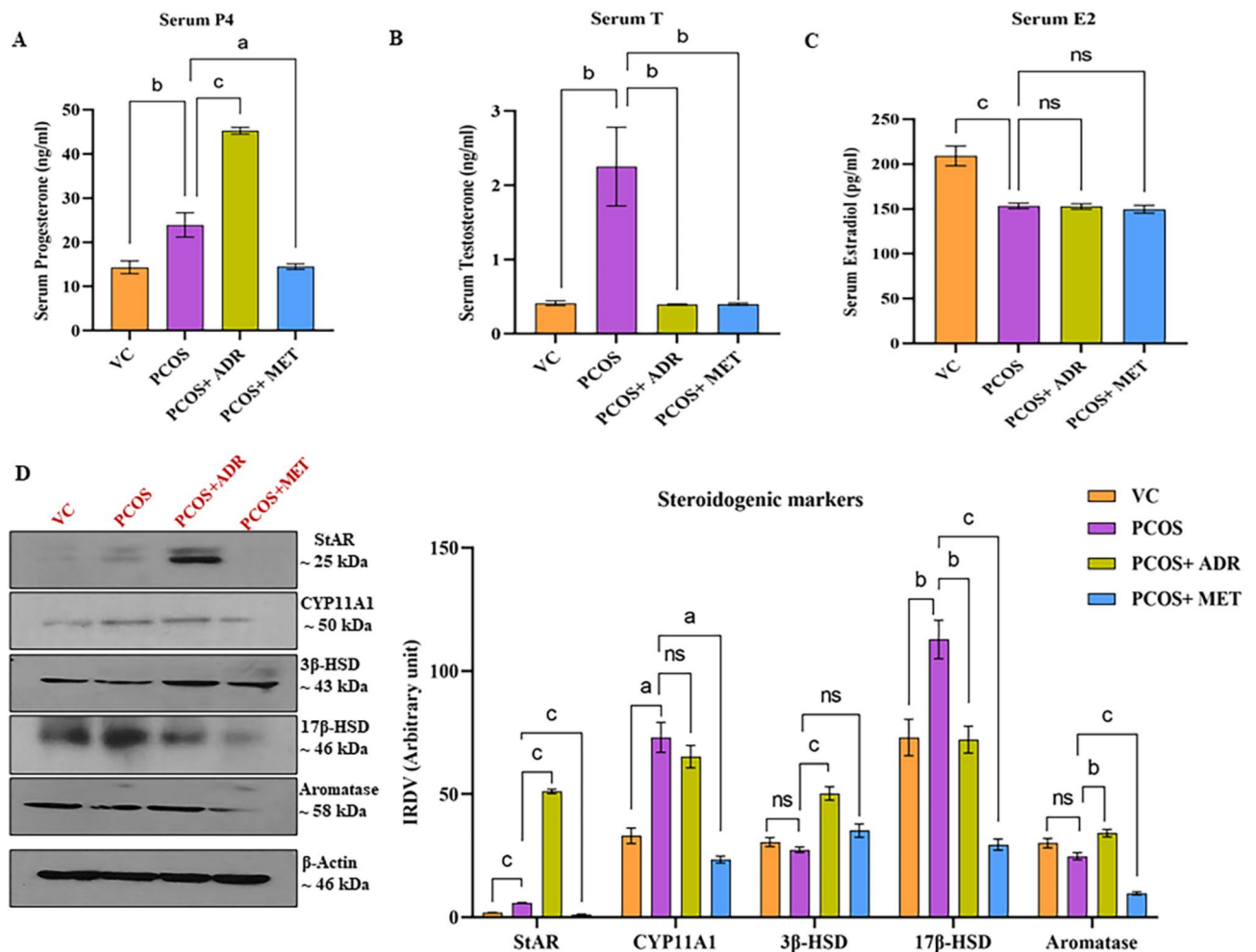


**Fig. 6.** Hormone levels and ovarian expression of steroidogenic proteins in different experimental groups. Circulating (A) progesterone, (B) testosterone, and (C) estradiol concentration in the different groups of experiment. Data are expressed as mean  $\pm$  SEM ( $n = 10$ ), and were analyzed by one-way ANOVA followed by the post hoc Bonferroni test. (D) Representative immunoblots and densitometric analysis of ovarian steroidogenic proteins, namely steroidogenic acute regulatory protein (StAR), Cytochrome P450 11A1 (CYP11A1), 3 $\beta$ -hydroxysteroid dehydrogenase (3 $\beta$ -HSD), 17 $\beta$ -hydroxysteroid dehydrogenase (17 $\beta$ -HSD) and aromatase in different experimental groups. Data are expressed as IRDV  $\pm$  SEM ( $n = 3$ ), analyzed by one-way ANOVA followed by the post hoc Bonferroni test.  $\beta$ -actin is used to normalize the results of immunoblots. VC vehicle-treated control mice, PCOS polycystic mice, PCOS + ADR adropin-treated PCOS mice, PCOS + MET metformin-treated PCOS mice, IRDV integrated relative density value. <sup>a</sup> $p < 0.05$ ; <sup>b</sup> $p < 0.01$ ; <sup>c</sup> $p < 0.001$ ; ns—not significant.

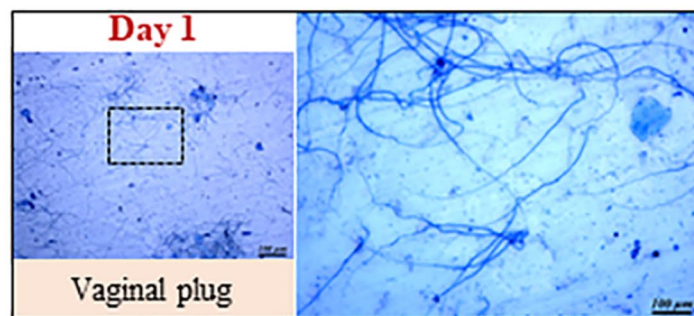
and embedded in paraffin wax. The ovary was serially sectioned at 6  $\mu$ m using a microtome (Leica, USA) and spread on gelatin-coated slides (Bancroft). The sections were further processed for histological analysis, immunohistochemistry, and TUNEL assay.

### Immunohistochemistry

The ovarian sections were processed through the standard protocol of immunohistochemistry<sup>32</sup>. After deparaffinization and rehydration, the slides were immersed in a solution of 3% H<sub>2</sub>O<sub>2</sub> in methanol for 30 min to inhibit the endogenous peroxidase activity of the tissue. Then, the slides were rinsed three times with 0.1 M PBS (pH 7.4) for 10 min. The non-specific background interactions were blocked by incubated the sections with normal goat serum for 2 h. Subsequently, the tissue sections were incubated with primary antibodies overnight at a temperature of 4  $^{\circ}$ C. The dilutions are listed in Table 2. Next morning, the slides were rinsed in 0.1 M PBS and then incubated with HRP-labeled secondary antibody for 2 h at room temperature. Afterwards, the slides were rinsed in 0.1 M PBS and treated with chromogenic substrate (3,3'-diaminobenzidine) (DAB; Vector). Finally, the sections were counterstained with hematoxylin, dehydrated, cleared, and mounted with DPX. The slides were examined under a light microscope (Nikon, Tokyo, Japan) and photographed.



A



B

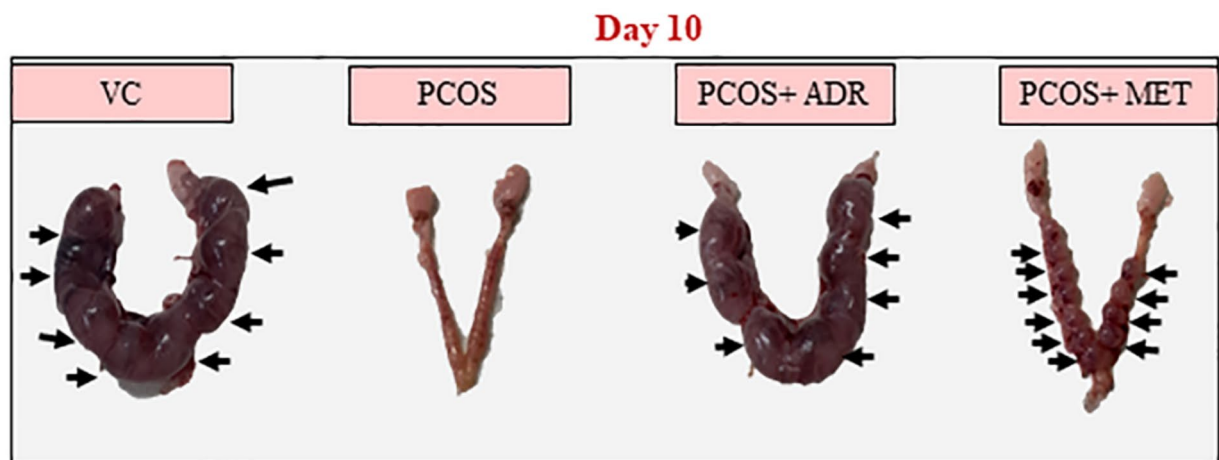


**Fig. 7.** Evaluation of fertility. **(A)** Vaginal plug of the mice showing the presence of spermatozoa, a sign of successful mating (Day 1). **(B)** Representative photographs of a mouse uterus showing implantation sites (Day 10) in different experimental groups. The arrowhead indicates implantation sites. VC vehicle-treated control mice, PCOS polycystic mice, PCOS + ADR adropin-treated PCOS mice, PCOS + MET metformin-treated PCOS mice.

S. No.	Antibody	Host species; class	Source	Catalogue no.	Dilutions
1	Adropin	Rabbit; Polyclonal	Sigma Aldrich	SAB3501053	1:500 (WB) 1:80 (IHC)
2	StAR	Rabbit; Polyclonal	Santa Cruz Biotechnology	SC 25,806	1:1000 (WB)
3	CYP11A1	Rabbit; Polyclonal	Cell Signaling Technology, Inc.	14,217	1:1000 (WB)
4	3 $\beta$ -HSD	Rabbit; Polyclonal	Thermo Fisher Scientific Inc.	PA5- 27,791	1:800 (WB)
5	17 $\beta$ -HSD	Rabbit; Polyclonal	Thermo Fisher Scientific Inc.	PA5-28065	1:800 (WB)
6	Aromatase	Rabbit; Polyclonal	Abcam	ab18995	1:800 (WB)
7	GPR19	Rabbit; Polyclonal	G Biosciences	ITA5843	1:500 (WB)
8	BAX	Rabbit; Polyclonal	Cell Signaling Technology, Inc	2772	1:800 (WB)
9	BCL2	Rabbit; Monoclonal	Cell Signaling Technology, Inc	3498	1:800 (WB)
10	Caspase 3	Rabbit; Polyclonal	Cell Signaling Technology, Inc	9661	1:800 (WB)
11	PCNA	Rabbit; Polyclonal	Thermo Fisher Scientific Inc.	PA1-38424	1:800 (WB) 1:100 (IHC)
12	$\beta$ -Actin	Mouse; Monoclonal HRP-tagged	Sigma Aldrich	A3854	1: 50,000 (WB)
13	Rabbit IgG	Goat	GeNei	1,140,380,011,730	1:4000 (WB)

**Table 2.** List of antibodies utilized in Immunoblot analyses and immunohistochemistry. StAR Steroidogenic acute regulatory protein, CYP11A1 Cytochrome P450 11A1, 3 $\beta$ -HSD 3 beta-hydroxysteroid dehydrogenase, 17 $\beta$ -HSD 17 beta-hydroxysteroid dehydrogenase, GPR19 G Protein-coupled receptor 19, BAX Bcl2-associated X protein, BCL2 B-cell leukemia/lymphoma 2, PCNA Proliferating cell nuclear antigen, Caspase 3 Cysteine aspartic acid protease 3.

### Terminal Deoxynucleotidyl transferase-mediated dUTP Nick end labeling (TUNEL) assay

Apoptosis was assessed by in situ 3'-OH end labeling of broken DNA fragments using the TUNEL apoptosis kit (catalog no: E-CK-A331, Elabscience Biotechnology Inc., Texas, USA). The paraffin-embedded ovarian histological sections of VC, PCOS, PCOS + ADR, and PCOS + MET groups were processed according to the manufacturer's protocol. After deparaffinization and rehydration, the ovarian sections were rinsed in 0.1 M PBS and treated with proteinase K for 20 minutes at 37°C. Thereafter, the sections were rinsed three times with 0.1 M PBS and incubated with a blocking buffer (3% H<sub>2</sub>O<sub>2</sub> in methanol) for 20 minutes to prevent endogenous tissue peroxidase activity. Subsequently, the sections were treated with TdT enzyme working solution, which consisted of TdT equilibrium buffer (40 µl), Biotin-dUTP (5 µl), and TdT enzyme (5 µl), at 37°C for 1 hour in a humidified dark chamber. Following three washes with 0.1 M PBS, the sections were exposed to streptavidin-HRP solution at 37°C for 30 minutes in a humidified dark chamber. Thereafter, the sections were rinsed with 0.1 M PBS and treated with the chromogenic reagent 3,3'-Diaminobenzidine (DAB) for 3–5 min. After washing with 0.1 M PBS, the sections were counterstained with hematoxylin, dehydrated with increasing series of ethanol (50%, 70%, 90%, and absolute), cleared in xylene, and mounted in DPX. The sections were examined and photographs were taken under a light microscope (Nikon, Tokyo, Japan). Apoptotic cells were observed by DAB reaction, showing distinct dark brown colour.

### Immunoblot

Ovaries were pooled and 10% (w/v) homogenate was prepared by using suspension buffer (0.01 M Tris pH 7.6, 0.001 M ethylenediaminetetraacetic acid pH 8.0, 0.1 M sodium chloride, 1 µg/ml aprotinin, 100 µg/ml phenylmethanesulfonyl fluoride). An equal amount of protein (60 µg), as determined by the Bradford method<sup>57</sup>, was loaded and run onto a 10% SDS-PAGE gel. After that, the proteins were electrophoretically transferred from the gel to a polyvinylidene difluoride (PVDF) membrane (Millipore India Pvt. Ltd.) at 50 volts overnight at 4 °C. The membrane was blocked for 1 h using phosphate-buffered saline (0.01 M, pH 7.4; NaH<sub>2</sub>PO<sub>4</sub> 16 mM, Na<sub>2</sub>HPO<sub>4</sub> 64 mM, NaCl 154 mM, 0.02% Tween 20) containing 5% non-fat dried milk, followed by 3 h of incubation with primary antibody. The dilutions used in the experiment are listed in Table 2. Subsequently, the PVDF membrane was washed in 0.1 M PBS-Tween 20 and was subjected to 2 h of incubation with a secondary antibody. After three times rinsing with 0.1 M PBS-Tween 20, signals were detected on X-ray film utilizing an enhanced chemiluminescence kit (Biorad, USA). The immunoblots were repeated three times for each protein. Computer-assisted image analysis software ImageJ 1.53a version (<https://imagej.net/ij/>) was used to perform densitometry. The bands were normalized to β-Actin. The data were presented as mean of the integrated density value ± SEM.

### Statistical analysis

All the statistical analyses were performed using GraphPad Prism 7 version (<https://www.graphpad.com/ma/in/login/?returnUrl=/myaccount/>). Data were presented as mean or IRDV ± SEM. The significant difference between VC and PCOS groups was analyzed by unpaired t-test. The differences between in vivo experimental groups were assessed by one-way ANOVA, followed by a post-hoc Bonferroni test.  $p < 0.05$  was considered statistically significant.

### Data availability

The datasets generated and/or analyzed during the present study are not publicly available but are available from the corresponding author on reasonable request.

Received: 17 October 2024; Accepted: 5 March 2025

Published online: 13 March 2025

### References

1. Yildiz, B. O., Bozdag, G., Yapici, Z., Esinler, I. & Yarali, H. Prevalence, phenotype and cardiometabolic risk of polycystic ovary syndrome under different diagnostic criteria. *Hum. Reprod. (Oxf.)* **27**, 3067–3073. <https://doi.org/10.1093/humrep/des232> (2012).
2. Escobar-Morreale, H. F. Polycystic ovary syndrome: definition, aetiology, diagnosis and treatment. *Nat. Rev. Endocrinol.* **14**, 270–284. <https://doi.org/10.1038/nrendo.2018.24> (2018).
3. Dumesic, D. A. et al. Scientific statement on the diagnostic criteria, epidemiology, pathophysiology, and molecular genetics of polycystic ovary syndrome. *Endocr. Rev.* **36**, 487–525 (2015). (DOI 10.1210/er.2015–1018).
4. Shorakae, S., Boyle, J. & Teede, H. Polycystic ovary syndrome: a common hormonal condition with major metabolic sequelae that physicians should know about. *Int. Med. J.* **44**, 720–726. <https://doi.org/10.1111/imj.12495> (2014).
5. Moran, L. J., Norman, R. J. & Teede, H. J. Metabolic risk in PCOS: phenotype and adiposity impact. *Trends Endocrinol. Metab.* **26**, 136–143. <https://doi.org/10.1016/j.tem.2014.12.003> (2015).
6. ESHRE/ASRM. Revised 2003 consensus on diagnostic criteria and long-term health risks related to polycystic ovary syndrome (PCOS). *Hum. Reprod.* **19**, 41–47. <https://doi.org/10.1093/humrep/deh098> (2004).
7. Huber-Buchholz, M. M., Carey, D. G. & Norman, R. J. Restoration of reproductive potential by lifestyle modification in obese polycystic ovary syndrome: role of insulin sensitivity and luteinizing hormone. *J. Clin. Endocrinol. Metab.* **84**, 1470–1474. <https://doi.org/10.1210/jcem.84.4.5596> (1999).
8. Rababa'h, A. M., Matani, B. R. & Yehya, A. An update of polycystic ovary syndrome: causes and therapeutics options. *Heliyon* **8**, e11010. <https://doi.org/10.1016/j.heliyon.2022.e11010> (2022 October 10).
9. Velazquez, E. M., Mendoza, S., Hamer, T., Sosa, F. & Glueck, C. J. Metformin therapy in polycystic ovary syndrome reduces hyperinsulinemia, insulin resistance, hyperandrogenemia, and systolic blood pressure, while facilitating normal menses and pregnancy. *Metabolism* **43**, 647–654 (1994). (DOI 10.1016/0026-0495(94)90209-7).
10. Glueck, C. J., Wang, P., Fontaine, R., Tracy, T. & Sieve-Smith, L. Metformin to restore normal menses in oligo-amenorrheic teenage girls with polycystic ovary syndrome (PCOS)11 The full text of this article is available via JAH Online at <http://www.elsevier.com/locate/jahonline>. *J. Adolesc. Health* **29**, 160–169 (2001). [https://doi.org/10.1016/S1054-139X\(01\)00202-6](https://doi.org/10.1016/S1054-139X(01)00202-6).



11. Tang, T., Lord, J. M., Norman, R. J., Yasmin, E. & Balen, A. H. Insulin-sensitising drugs (metformin, Rosiglitazone, Pioglitazone, D-chiro-inositol) for women with polycystic ovary syndrome, oligo amenorrhoea and subfertility. *Cochrane Database Syst. Rev.* **5**, CD003053. <https://doi.org/10.1002/14651858.CD003053.pub5> (2012).
12. Toulis, K. A. et al. Adiponectin levels in women with polycystic ovary syndrome: A systematic review and a meta-analysis. *Hum. Reprod. Update.* **15**, 297–307. <https://doi.org/10.1093/humupd/dmp006> (2009).
13. Munir, I. et al. Resistin stimulation of 17 $\alpha$ -hydroxylase activity in ovarian theca cells in vitro: relevance to polycystic ovary syndrome. *J. Clin. Endocrinol. Metab.* **90**, 4852–4857 (2005). (DOI 10.1210/jc.2004–2152).
14. Baldani, D. P. et al. Altered leptin, adiponectin, resistin and Ghrelin secretion May represent an intrinsic polycystic ovary syndrome abnormality. *Gynecol. Endocrinol.* **35**, 401–405. <https://doi.org/10.1080/09513590.2018.1534096> (2019).
15. Chan, T. F. et al. Increased plasma visfatin concentrations in women with polycystic ovary syndrome. *Fertil. Steril.* **88**, 401–405. <https://doi.org/10.1016/j.fertnstert.2006.11.120> (2007).
16. Panidis, D. et al. Plasma visfatin levels in normal weight women with polycystic ovary syndrome. *Eur. J. Intern. Med.* **19**, 406–412. <https://doi.org/10.1016/j.ejim.2007.05.014> (2008).
17. Tan, B. K. et al. Metformin treatment May increase omentin-1 levels in women with polycystic ovary syndrome. *Diabetes* **59**, 3023–3031. <https://doi.org/10.2337/db10-0124> (2010).
18. Orlík, B. et al. Plasma omentin and adiponectin levels as markers of adipose tissue dysfunction in normal weight and obese women with polycystic ovary syndrome. *Clin. Endocrinol. (Oxf.)* **81**, 529–535. <https://doi.org/10.1111/cen.12381> (2014).
19. Tan, B. K. et al. Insulin and Metformin regulate Circulating and adipose tissue chemerin. *Diabetes* **58**, 1971–1977. <https://doi.org/10.2337/db08-1528> (2009).
20. Bozaoglu, K. et al. Chemerin is associated with metabolic syndrome phenotypes in a Mexican-American population. *J. Clin. Endocrinol. Metab.* **94**, 3085–3088 (2009). (DOI 10.1210/jc.2008–1833).
21. Roche, J. et al. Apelin (APLN) and Apelin receptor (APLNR) in human ovary: expression, signaling, and regulation of steroidogenesis in primary human luteinized granulosa cells. *Biol. Reprod.* **95**, 104. <https://doi.org/10.1095/biolreprod.116.141754> (2016).
22. Kumar, K. G. et al. Identification of Adropin as a secreted factor linking dietary macronutrient intake with energy homeostasis and lipid metabolism. *Cell. Metab.* **8**, 468–481. <https://doi.org/10.1016/j.cmet.2008.10.011> (2008).
23. Ganesh-Kumar, K. G. et al. Adropin deficiency is associated with increased adiposity and insulin resistance. *Obesity* **20**, 1394–1402. <https://doi.org/10.1038/oby.2012.31> (2012).
24. Gao, S. et al. Therapeutic effects of Adropin on glucose tolerance and substrate utilization in diet-induced obese mice with insulin resistance. *Mol. Metab.* **4**, 310–324. <https://doi.org/10.1016/j.molmet.2015.01.005> (2015 April 1).
25. Thapa, D. et al. Adropin reduces blood glucose levels in mice by limiting hepatic glucose production. *Physiol. Rep.* **7**, e14043. <https://doi.org/10.14814/phy2.14043> (2019).
26. Altamimi, T. R. et al. Adropin regulates cardiac energy metabolism and improves cardiac function and efficiency. *Metabolism* **98**, 37–48. <https://doi.org/10.1016/j.metabol.2019.06.005> (2019).
27. Jasaszwili, M. et al. Effects of Adropin on proliferation and differentiation of 3T3-L1 cells and rat primary preadipocytes. *Mol. Cell. Endocrinol.* **496**, 110532. <https://doi.org/10.1016/j.mce.2019.110532> (2019).
28. Tripathi, S., Maurya, S. & Singh, A. Adropin May promote insulin stimulated steroidogenesis and spermatogenesis in adult mice testes. *J. Exp. Zool. Pt A.* **341**, 86–98. <https://doi.org/10.1002/jez.2763> (2024).
29. Tripathi, S., Maurya, S. & Singh, A. Adropin, a novel hepatokine: localization and expression during postnatal development and its impact on testicular functions of pre-pubertal mice. *Cell. Tissue Res.* **395**, 171–187. <https://doi.org/10.1007/s00441-023-03852-9> (2024).
30. Tripathi, S., Maurya, S. & Singh, A. Adropin promotes testicular functions by modulating redox homeostasis in adult mouse. *Endocrine* **86**, 428–440. <https://doi.org/10.1007/s12020-024-03921-1> (2024).
31. Maurya, S., Tripathi, S., Arora, T. & Singh, A. Adropin May regulate corpus luteum formation and its function in adult mouse ovary. *Hormones* **22**, 725–739. <https://doi.org/10.1007/s42000-023-00476-0> (2023).
32. Maurya, S., Tripathi, S. & Singh, A. Ontogeny of Adropin and its receptor expression during postnatal development and its progonadal role in the ovary of pre-pubertal mouse. *J. Steroid Biochem. Mol. Biol.* **234**, 106404. <https://doi.org/10.1016/j.jsbmb.2023.106404> (2023).
33. Maurya, S., Tripathi, S., Arora, T. & Singh, A. Adropin May regulate ovarian functions by improving antioxidant potential in adult mouse. *J. Steroid Biochem. Mol. Biol.* **242**, 106524. <https://doi.org/10.1016/j.jsbmb.2024.106524> (2024).
34. Bousmpoula, A. et al. Adropin levels in women with polycystic ovaries undergoing ovarian stimulation: correlation with lipoprotein lipid profiles. *Gynecol. Endocrinol.* **34**, 153–156. <https://doi.org/10.1080/09513590.2017.1379498> (2018).
35. Kume, T. et al. A possible connection between tumor necrosis factor alpha and Adropin levels in polycystic ovary syndrome. *J. Endocrinol. Investig.* **39**, 747–754. <https://doi.org/10.1007/s40618-016-0453-5> (2016).
36. Gao, S. et al. The peptide hormone Adropin regulates signal transduction pathways controlling hepatic glucose metabolism in a mouse model of diet-induced obesity. *J. Biol. Chem.* **294** (36), 13366–13377. <https://doi.org/10.1074/jbc.RA119.008967> (2019).
37. Sanchez-Garrido, M. A. & Tena-Sempere, M. Metabolic dysfunction in polycystic ovary syndrome: pathogenic role of androgen excess and potential therapeutic strategies. *Mol. Metab.* **35**, 100937. <https://doi.org/10.1016/j.molmet.2020.01.001> (2020).
38. Azziz, R. et al. The androgen excess and PCOS society criteria for the polycystic ovary syndrome: the complete task force report. *Fertil. Steril.* **91**, 456–488. <https://doi.org/10.1016/j.fertnstert.2008.06.035> (2009).
39. Huang, A., Brennan, K. & Azziz, R. Prevalence of hyperandrogenemia in the polycystic ovary syndrome diagnosed by the National institutes of health 1990 criteria. *Fertil. Steril.* **93**, 1938–1941. <https://doi.org/10.1016/j.fertnstert.2008.12.138> (2010).
40. Nakamura, Y. et al. Type 5 17 $\beta$ -hydroxysteroid dehydrogenase (AKR1C3) contributes to testosterone production in the adrenal reticularis. *J. Clin. Endocrinol. Metab.* **94**, 2192–2198 (2009 June) (DOI 10.1210/jc.2008–2374).
41. Kim, J., Bagchi, I. C. & Bagchi, M. K. Control of ovulation in mice by progesterone receptor-regulated gene networks. *Mol. Hum. Reprod.* **15**, 821–828. <https://doi.org/10.1093/molehr/gap082> (2009).
42. Teede, H. J., Hutchison, S. K. & Zoungas, S. The management of insulin resistance in polycystic ovary syndrome. *Trends Endocrinol. Metab.* **18**, 273–279. <https://doi.org/10.1016/j.tem.2007.08.001> (2007).
43. Rice, S., Pellatt, L., Ramanathan, K., Whitehead, S. A. & Mason, H. D. October 1. Metformin inhibits aromatase via an extracellular signal-regulated kinase-mediated pathway. *Endocrinology* **150**, 4794–4801 (DOI 10.1210/en.2009–0540) (2009).
44. Shah, M. Z. & Shrivastava, V. K. Ameliorative effects of Quercetin on endocrine and metabolic abnormalities associated with experimentally induced polycystic ovary syndrome in mice. *Comp. Clin. Pathol.* **32**(3), 383–391 (2023 Jun).
45. ul haq Shah, M. Z., Shrivastava, V. K., Mir, M. A. & Olaniyi, K. S. Role of diacerein on steroidogenesis and folliculogenesis related genes in ovary of letrozole-induced PCOS mice. *Chemico-Biol. Interact.* **25**, 377(110468) (2023 May).
46. Shah, M. Z. et al. Effect of Quercetin on steroidogenesis and folliculogenesis in ovary of mice with experimentally-induced polycystic ovarian syndrome. *Front. Endocrinol.* **24**, 14(1153289) (2023 Apr).
47. ul haq Shah, M. Z., Shrivastava, V. K., Muzamil, S. & Olaniyi, K. S. Diacerein mitigates endocrine and cardio-metabolic disruptions in experimental PCOS mice model by modulating AdipoR1/PON 1. *BMC Endocr. Disorders* **10**, 24 (109) (2024 Jul).
48. Shah, M. Z. et al. Chlorogenic acid restores ovarian functions in mice with letrozole-induced polycystic ovarian syndrome via modulation of adiponectin receptor. *Biomedicine* **14**, 11(3):900 (2023 Mar).
49. ul haq Shah, M. Z., Shrivastava, V. & Mir, M. A. Metformin treatment ameliorates endocrine-metabolic disturbances in letrozole-induced PCOS mice model by modulating adiponectin status. *Obes. Med.* **1**, 31:100392 (2022 May).

50. Palomba, S. et al. Metformin administration versus laparoscopic ovarian diathermy in clomiphene citrate-resistant women with polycystic ovary syndrome: a prospective parallel randomized double-blind placebo-controlled trial. *J. Clin. Endocrinol. Metab.* **89**, 4801–4809 (2004). (DOI 10.1210/jc.2004–0689).
51. Kumariya, S., Ubba, V., Jha, R. K. & Gayen, J. R. Autophagy in ovary and polycystic ovary syndrome: role, dispute and future perspective. *Autophagy* **17**, 2706–2733. <https://doi.org/10.1080/15548627.2021.1938914> (2021).
52. Li, X. et al. The role of androgen in autophagy of granulosa cells from PCOS. *Gynecol. Endocrinol.* **35**, 669–672. <https://doi.org/10.1080/09513590.2018.1540567> (2019).
53. Pandey, V. et al. Role of oxidative stress and low-grade inflammation in letrozole-induced polycystic ovary syndrome in the rat. *Reprod. Biol.* **16**, 70–77. <https://doi.org/10.1016/j.repbio.2015.12.005> (2016).
54. Parikha, Singh, P. J. & Krishna, A. Anti-hyperglycaemic activity of Tribulus terrestris fruit extract restores metabolic imbalance in letrozole induced -PCOS mice. *J. Pharmacogn. Phytochem.* **11**, 304–311 (2019).
55. Gao, S. et al. Regulation of substrate oxidation preferences in muscle by the peptide hormone Adropin. *Diabetes* **63**, 3242–3252. <https://doi.org/10.2337/db14-0388> (2014).
56. Elia, E., Sander, V. & Luchetti, C. G. The mechanisms involved in the action of Metformin in regulating ovarian function in hyperandrogenized mice. *Mol. Hum. Reprod.* **12**, 475–481. <https://doi.org/10.1093/molehr/gal057> (2006).
57. Bradford, M. M. A rapid and sensitive method for the quantitation of microgram quantities of protein utilizing the principle of protein utilizing the principle of protein-dye binding. *Anal. Biochem.* **72**, 248–254. <https://doi.org/10.1006/abio.1976.9999> (1976).

## Acknowledgements

S.M. and S.T. highly acknowledge CSIR, New Delhi, for the grant as JRF and SRF. DST-FIST and UGC-CAS program to the Department of Zoology, BHU, is acknowledged.

## Author contributions

S.M. and S.T. contributed equally in the collection of data, performed all the experiments, prepared figures and graphs, and writing, revising the manuscript. T. A. conceptualized and reviewed the manuscript. A.S. conceptualized, supervised, reviewed the work, and edited the final draft. A.S. All the authors, read and agreed to publish the final manuscript.

## Funding

This work was financially supported by bridge grant (SRICC/Bridge Grant/2023-24/8135) under Institute of eminence scheme, BHU.

## Declarations

## Competing interests

The authors declare no competing interests.

## Additional information

**Supplementary Information** The online version contains supplementary material available at <https://doi.org/10.1038/s41598-025-93215-x>.

**Correspondence** and requests for materials should be addressed to A.S.

**Reprints and permissions information** is available at [www.nature.com/reprints](http://www.nature.com/reprints).

**Publisher's note** Springer Nature remains neutral with regard to jurisdictional claims in published maps and institutional affiliations.

**Open Access** This article is licensed under a Creative Commons Attribution-NonCommercial-NoDerivatives 4.0 International License, which permits any non-commercial use, sharing, distribution and reproduction in any medium or format, as long as you give appropriate credit to the original author(s) and the source, provide a link to the Creative Commons licence, and indicate if you modified the licensed material. You do not have permission under this licence to share adapted material derived from this article or parts of it. The images or other third party material in this article are included in the article's Creative Commons licence, unless indicated otherwise in a credit line to the material. If material is not included in the article's Creative Commons licence and your intended use is not permitted by statutory regulation or exceeds the permitted use, you will need to obtain permission directly from the copyright holder. To view a copy of this licence, visit <http://creativecommons.org/licenses/by-nc-nd/4.0/>.

© The Author(s) 2025